ELSEVIER

Ultramicroscopy 88 (2001) 187–194

ultramicroscopy

www.elsevier.nl/locate/ultramic

# Image-spectroscopy–II. The removal of plural scattering from extended energy-filtered series by *Fourier* deconvolution

P.J. Thomas, P.A. Midgley*

*Department of Materials Science and Metallurgy, University of Cambridge, Pembroke Street, Cambridge, CB2 3QZ, UK*

Received 7 August 2000; received in revised form 28 December 2000

**Abstract**

The increased spectral information obtained by acquiring an EFTEM image-series over several hundred eV allows plural scattering to be removed from loss images using standard deconvolution techniques developed for the quantification of EEL spectra. In this work, both *Fourier*-log and *Fourier*-ratio deconvolution techniques have been applied successfully to such image-series. Application of the *Fourier*-log technique over an energy-loss range of several hundred eV has been achieved by implementation of a novel method that extends the effective dynamic range of EFTEM image-series acquisition by over four orders of magnitude. Experimental results show that the removal of plural scattering from EFTEM image-series gives a significant improvement in quantification for thicker specimen regions. Further, the recovery of the single-scattering distribution using the *Fourier*-log technique over an extended energy-loss range is shown to result in an increase in both the ionisation-edge jump-ratio and the signal-to-noise ratio.


## 1. Introduction

Electron spectroscopic imaging (ESI) in the energy-filtered TEM (EFTEM) provides a valuable tool for the rapid mapping of chemical distribution at the nanometre level. A relatively new approach in EFTEM analysis, termed 'image-spectroscopy', involves the acquisition of an extended image-series [1,2]. Typically, tens of images are recorded sequentially across several hundred eV loss to create a three dimensional dataset containing (serially-acquired) spectral information in addition to spatially parallel data. This approach offers numerous advantages over conventional two- or three-window methods and, as outlined in the preceding paper, such image-series may be treated as a two-dimensional array of 'image-spectra' whose energy resolution is determined by the acquisition step size. Techniques developed for the analysis of EEL spectra may therefore be applied directly to image-spectra [3] enabling, for example, plural scattering to be removed using *Fourier*-transform based deconvolution techniques.

It is well known that the removal of plural scattering from the EEL spectrum leads to an improvement in the quantitative analysis of thicker specimens, and allows core-loss edges of similar energy-loss to be separated more effectively [4,5]. Further, the retrieval of the single-scattering

*Corresponding author. Tel.: +1223-334561; fax: +1223-334567.

*E-mail address:* pam33@cam.ac.uk (P.A. Midgley).

0304-3991/01/$ - see front matter 
PII: S0304-3991(01)00078-X

distribution (SSD) from the low-loss spectrum gives rise to the possibility of quantitative elemental mapping using core-loss edges normally obscured by plural plasmon scattering events, for example the $M_{23}$ edges of the transition metals [6]. In this work, *Fourier*-ratio and *Fourier*-log deconvolution techniques have been applied to image-series, enabling the SSDs to be recovered from both low-loss and core-loss image-spectra.

## 2. *Fourier*-ratio deconvolution

*Fourier*-ratio deconvolution uses low-loss information as the 'deconvolution function', necessitating the acquisition of a low-loss image-series in addition to the core-loss data of interest. In principle, the SSD $I^1_{\text{core}}(E)$ may be recovered from the recorded spectral intensity by dividing the *Fourier*-transform (FT) of the core-loss spectrum $i_{\text{core}}(v)$ by the FT of the low-loss intensity, $i_{\text{low}}(v)$, and multiplying by a reconvolution function, $z(v)$ (for example, the FT of the zero-loss peak), giving [7]

$$i^1_{\text{core}}(v) = z(v)\frac{i_{\text{core}}(v)}{i_{\text{low}}(v)}. \quad (1)$$

*Fourier*-ratio deconvolution is well suited to energy-filtered image-series since the ratio of absolute intensity of the low-loss region relative to the core-loss series is not required, allowing problems concerning the limited dynamic range of the CCD detector to be avoided.

The validity of applying *Fourier*-ratio deconvolution to image-series can be demonstrated by calculating chemical concentration maps from a sample of known composition over varying thickness, $t$, using an image-series before and after deconvolution. In this example, the Cr $L_{23}$ edge is used to map a pure chromium wedge (Fig. 1a). The elemental volume density $C_{\text{Cr}}$ (in atoms per unit volume) may be calculated using the relationship [4]

$$C_{\text{Cr}} = \frac{I^1_{\text{Cr}}(\beta, \Delta)}{I_0(\beta)\sigma_{\text{Cr}}(\beta, \Delta)t} \approx \frac{I_{\text{Cr}}(\beta, \Delta)}{I_{\text{low}}(\beta, \Delta)\sigma_{\text{Cr}}(\beta, \Delta)t}, \quad (2)$$

where $I_{\text{Cr}}$ is the background-subtracted core-loss intensity, $I^1_{\text{Cr}}$ the corresponding SSD intensity, $I_0$ the zero-loss intensity and $I_{\text{low}}$ the corresponding low-loss intensity, captured over a scattering semi-angle $\beta$ and signal integration width $\Delta$. The term approximated in Eq. (2) represents the method commonly used for the correction of plural scattering, namely division with the corresponding low-loss signal. The middle term describes the more exact correction involving deconvolution, where the zero-loss intensity distribution is used to correct elastic effects. Following Eq. (2), if plural scattering, thickness variations and elastic scattering effects are removed correctly, a line-trace of the corresponding Cr concentration map over increasing $t$ should give a flat compositional profile.

Using a Philips CM300 equipped with a Gatan imaging filter (GIF), a core-loss series from 500 to 700 eV loss and the corresponding low-loss series from 0 to 150 eV were acquired, using an energy-step and slit width of 5 eV and an objective aperture semi-angle, $\beta = 10$ mrad. Elemental volume density maps were then calculated using the data both before and after *Fourier*-ratio deconvolution following Eq. (2). The resultant maps are shown in Fig. 1. As a pure chromium sample was analysed (with a little surface oxide), the inelastic mean free path $\lambda$ was assumed to be constant and thickness was corrected using the corresponding $t/\lambda$ map calculated from the low-loss data. The removal of plural scattering proved to be effective over the full thickness range investigated (from $0 < t < 2\lambda$), although the current software allows deconvolution up to $t/\lambda = \pi$ [8]. This may be illustrated by comparison of the line-traces of the Cr elemental composition maps calculated from the image-series both after *Fourier*-ratio deconvolution and using the conventional plural scattering correction, as shown in Fig. 1c with varying signal integration widths $\Delta$. The latter deviates with both increasing $t$ and $\Delta$, suggesting the low-loss correction over-estimate the plural scattering contribution. This over-estimation originates from the low-loss correction compensating for plural scattering intensity falling outside the signal integration region. In comparison, line-traces of the deconvolved compositional density map show relatively flat profiles beyond the region at the edge of the sample. This indicates that the removal of plural scattering by deconvolution results in an

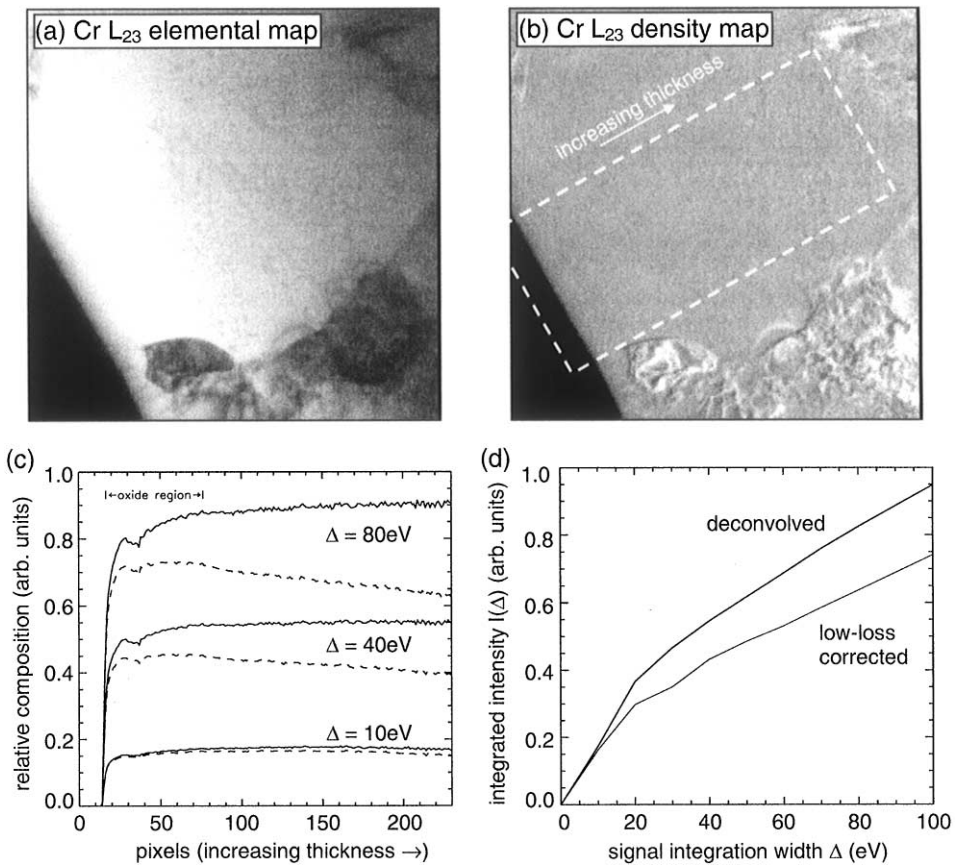


Fig. 1. *Fourier*-ratio deconvolution of an image series across the Cr $L_{23}$ edge. (a) Cr elemental map (deconvolved), with no corrections for thickness or elastic effects applied. (b) Compositional density map corrected for thickness and elastic scattering effects by division with the appropriate thickness and zero-loss images, respectively. (c) Comparison of compositional line-trace along the region marked in (a) with varying signal integration-width $\Delta$; plural scattering removed by *Fourier*-ratio deconvolution (solid) and low-loss correction (dashed). Thickness range is from $0 < t < 2\lambda$. (d) Integrated edge intensity plotted as a function of integration width, illustrating over-compensation of plural scattering using the low-loss correction for a thickness of $t/\lambda = 1$.

improvement in quantification for thicker specimens and larger integration regions. The degree of improvement may be illustrated by direct comparison of edge intensities integrated over various integration windows $I(\Delta)$ using both the deconvolved and low-loss corrected data. For a moderately large integration window (e.g. $\Delta = 60\,\text{eV}$), the deviation between the two methods at $t/\lambda \sim 1$ is over 30% (Fig. 1d).

Plural scattering events from inelastic processes before the core-loss series onset energy are not removed by *Fourier*-ratio deconvolution. In order to satisfy the continuity requirements for a *Fourier* series, the pre-edge background to the first ionisation edge is first removed using standard background removal methods [7]. Accordingly, only successive ionisation edges benefit from a reduced background contribution. This may be illustrated by calculation of signal-to-noise ratio (SNR) plots for the chromium edge before and after deconvolution, using the approach of Kothleitner and Hofer [9] based on the background confidence parameter ($h$) approach implemented by Egerton [10]. For the purpose of evaluating $h$ in the case of the deconvolved image-spectra, the pre-edge background removed prior to deconvolution

was used. As may be seen by comparison of the image-spectra shown in Figs. 2a and c, there is no significant improvement in the background to ionisation edge jump-ratio after *Fourier*-ratio deconvolution. Likewise, as shown in Figs. 2b and 2d, there is no significant change in the SNR for the deconvolved chromium $L_{23}$ image-spectrum ionisation edge compared with the as-recorded data, particularly for the small signal integration width required to produce quantitatively reliable results. It should be emphasised, however, that subsequent ionisation edges should show an improvement in both jump-ratio and SNR as a result of a decrease in their pre-edge backgrounds (see the following section). In order to receive the full benefit of plural scattering removal, it is therefore necessary to retrieve the single-scattering distribution using a more complete deconvolution method; for example, *Fourier*-log deconvolution.

## 3. *Fourier*-log deconvolution

The *Fourier*-log approach requires no deconvolution function, instead utilising the Poisson statistics of plural scattering to recover the SSD $I^1(E)$ using a logarithmic relation of the form [11]

$$i^1(v) = z(v)\ln\left[\frac{i(v)}{z(v)}\right], \tag{3}$$

where $i(v)$ is the *Fourier*-transform of the recorded spectrum from zero-loss to beyond the highest core-loss of interest. The requirement for spectral

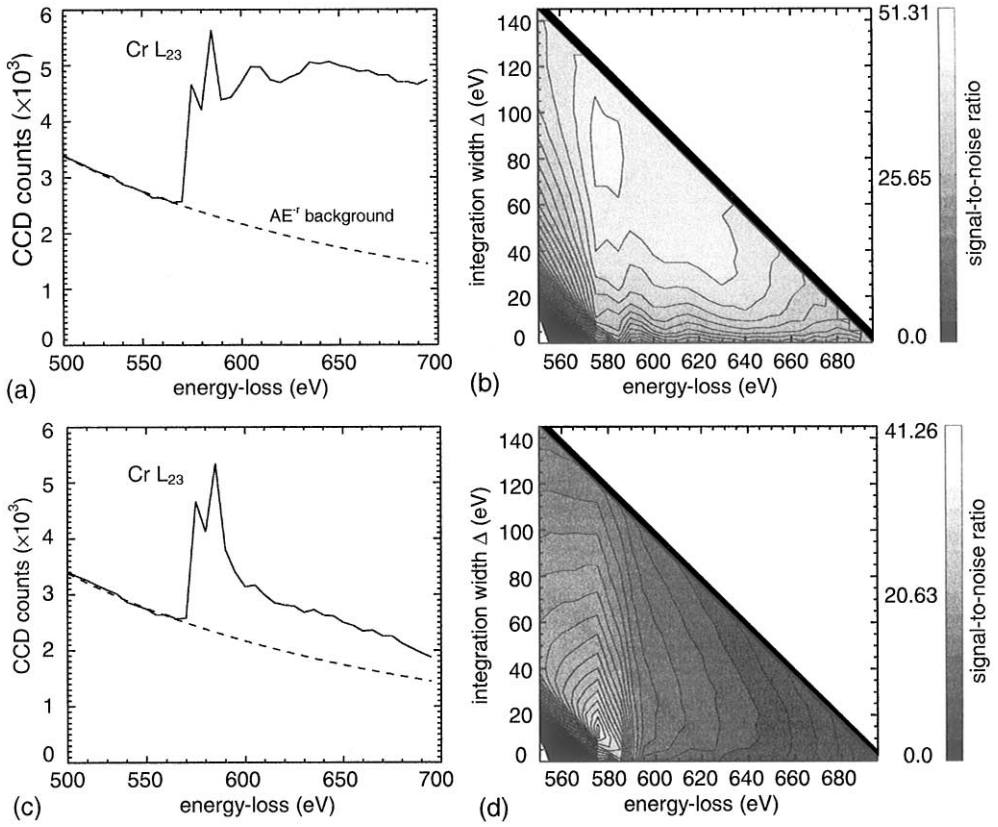


Fig. 2. Image-spectra extracted from a Cr $L_{23}$ image-series with corresponding signal to noise ratio plots following the approach of Kothleitner and Hofer [8], calculated (a, b) before and (c, d) after removal of plural-scattering using *Fourier*-ratio deconvolution. The background contribution to the deconvolved spectrum has been replaced for comparison. The plots show no significant change in SNR for a small energy window between as-recorded and deconvolved spectra.

information over such an extensive range poses a significant problem for EFTEM image-series acquisition, placing unrealistic demands on the dynamic range of the CCD camera. While image-series may be recorded over a considerable energy-loss range with good counting

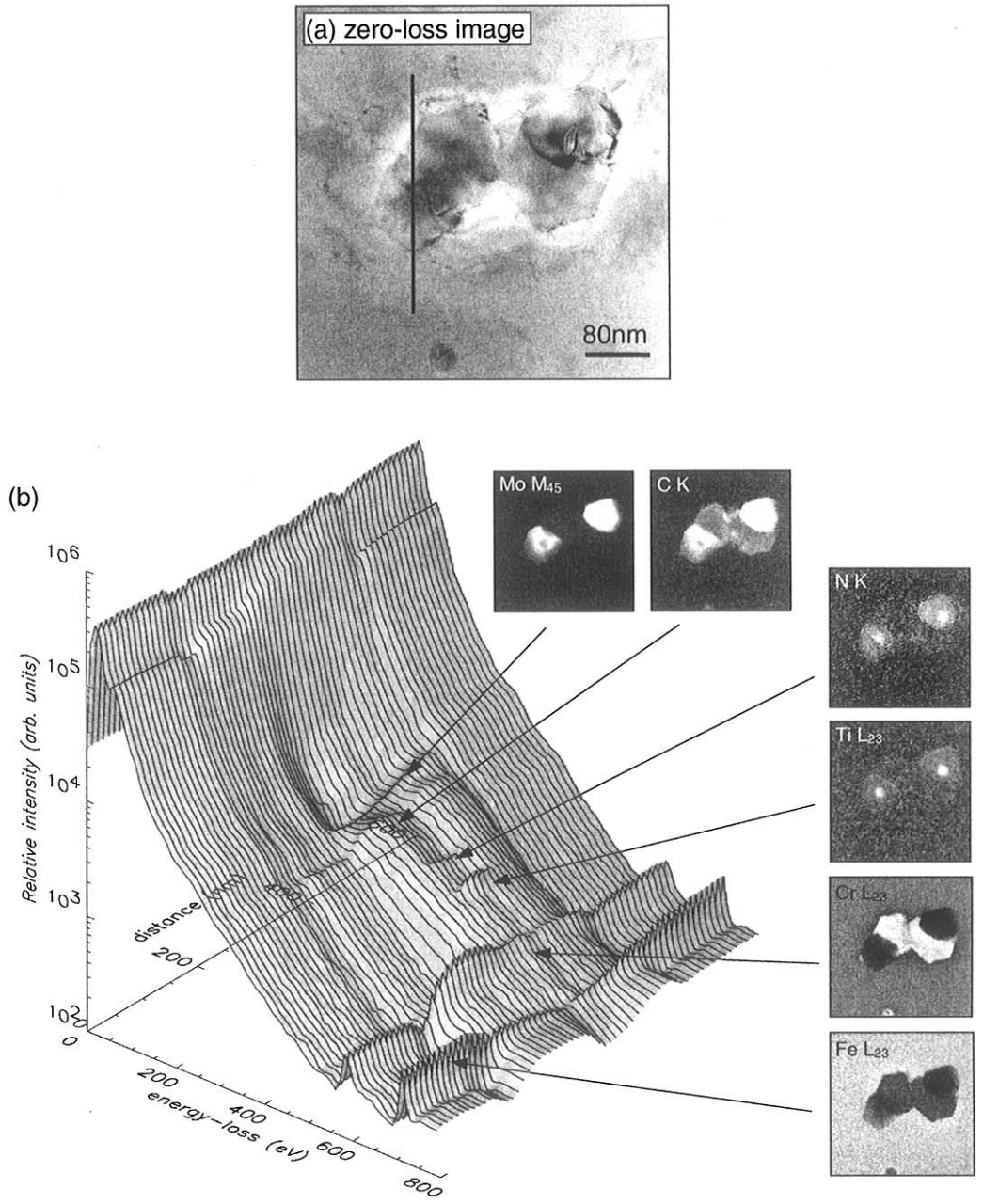


Fig. 3. (a) Zero-loss image of a precipitate cluster from a series of 80 images acquired from a 316-type stainless steel. (b) An image-spectrum line trace across the line marked in (a), illustrating the extended dynamic range obtained by dynamically varying image integration times and pixel binning. A number of core-loss edges, acquired within the series, are revealed.

statistics at high losses, ultimately the dynamic range of the CCD camera restricts the acquisition energy range, particularly within the low-loss region where large variations in intensity can occur.

A method has been developed that increases the effective dynamic range of the CCD detector by over four orders of magnitude [12]. By dynamically adjusting exposure times and detector hardware binning between successive acquisitions, the ratio between the energy-loss signal and the statistical detector noise may be optimised throughout the image-series. A computer program written in the Digital Micrograph script language [13] allows acquisition in an automated manner by evaluating the intensity of the previously captured image to modify subsequent acquisition parameters. Post acquisition, corrections are made to take into account any change in exposure time before storing data directly to a computer hard drive for further analysis.

The technique is demonstrated by analysis of a precipitate cluster in a 316-type stainless steel (Fig. 3a). An image-series consisting of 80 images was acquired, using a Philips CM300 FEGTEM equipped with a Gatan imaging filter, from zero-loss to 800 eV loss, with an energy-step and energy-selecting slit width of 10 eV and an objective aperture semi-angle, $\beta = 10$ mrad. Acquisition time for the entire image-series was less

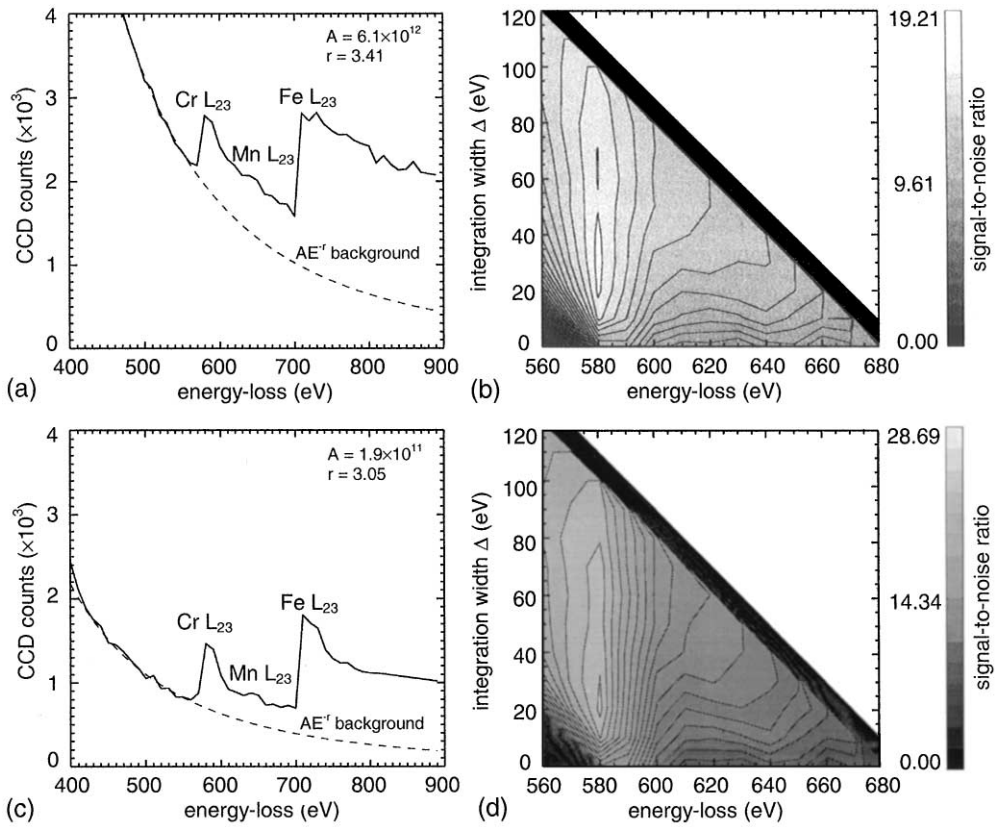


Fig. 4. SNR calculations for the Cr $L_{23}$ edge from image-spectra extracted from a 316 stainless steel image-series, local sample thickness $t/\lambda \sim 0.8$ (a) Extracted image-spectrum, not corrected for plural scattering. The lower loss region is not shown. (b) Corresponding SNR plot, using a power-law relationship over a background-fitting region of 500–570 eV. (c) Image-spectrum after *Fourier*-log deconvolution, showing a smaller background contribution and lower background fitting parameters, $A$ and $r$. (d) The SNR plot for the deconvolved image-spectrum, showing a significant improvement over the unprocessed data.

than ten minutes. *Post-facto* spectral analysis of the dataset reveals a number of core-loss edges captured within the single acquisition, as illustrated by the (deconvolved) image-spectrum line-trace across the precipitate cluster shown in Fig. 3b, and contains some species thought previously to be absent.

Extracted image-spectra before and after deconvolution are shown in Fig. 4. *Fourier*-log deconvolution of the image-series proved to be successful, resulting in reduced background contribution for all edges within the series despite the relatively thin local sample thickness ($t/\lambda \approx 0.45$ at 300 keV). This reduction in background contribution results in a significant increase in the jump-ratio as shown in Figs. 4a and c, where the chromium $L_{23}$ edge shows an increase of over 30% in the jump-ratio after deconvolution. Further, the reduced background contribution leads to a shallower pre-edge slope, resulting in a reduction in both the scaling constant $A$ and slope exponent $r$ of the fitted $AE^{-r}$ power law background. Minimising these factors leads to a reduction in the background fit confidence parameter, resulting in an improvement in the ionisation edge signal-to-noise ratio. For the image-spectrum shown in Fig. 4, the background confidence parameter for the chromium $L_{23}$ edge was reduced from $h \approx 5$ (as-recorded) to $h \approx 2$ after deconvolution. The effect of this reduction in $h$ is shown in the SNR plots of Figs. 4b and 4d, where the signal to noise ratio for the chromium $L_{23}$ edge increases from $\approx$

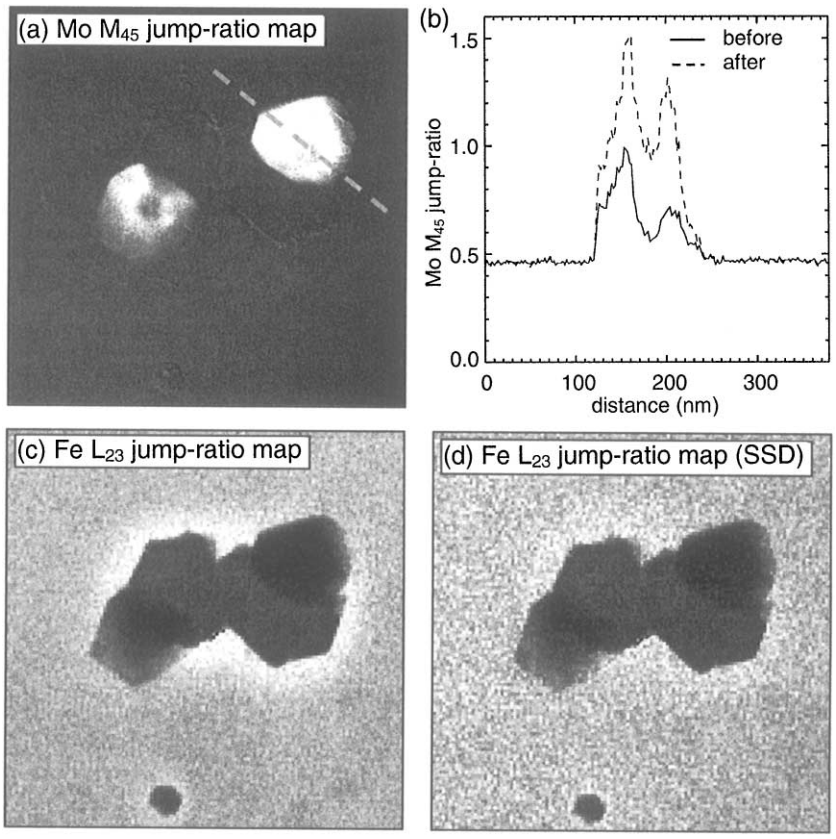


Fig. 5. (a, b) The increase in jump-ratio resulting from deconvolution may be conveniently illustrated by a jump-ratio line-trace. Comparison for the Mo $M_{45}$ jump-ratio map (a) before and (b) after deconvolution shows a 50% increase in jump-ratio. (c, d) Fe $L_{23}$ jump-ratio maps both before and after *Fourier*-log deconvolution. Thickness effects are removed substantially by deconvolution, most noticeably in the preferentially thinned area around the precipitates.

19 (as-recorded) to $\approx 29$ after deconvolution. Since the uncertainty in recorded intensity is a result of statistical fluctuations in the CCD detector, care was taken to ensure the *unprocessed* information was used to calculate the standard deviation $\sigma$ when calculating $h$ for the *Fourier*-log deconvolved data. In terms of elemental mapping, this reduction in $h$ and increase in SNR allows quantitative chemical distribution maps to be calculated with lower noise content and higher confidence levels.

Jump-ratio images calculated using the deconvolved image series show an amplified noise content when compared with the unprocessed maps, as a result of dividing the relatively unchanged post-edge image after deconvolution with a pre-edge image of decreased intensity but unchanged statistical fluctuation. However, image contrast is improved as a result of an increase in jump-ratio. This is shown for the molybdenum $M_{45}$ edge in Fig. 5a by means of a jump-ratio line-trace in Fig. 5b, where the jump-ratio increases by approximately 50% after deconvolution. In addition, recovery of the SSD produces jump-ratio images where sample thickness effects are substantially less than in their as-recorded counterparts. This may be observed at the preferentially thinned region surrounding the precipitate cluster in the deconvolved iron $L_{23}$ jump-ratio image (Figs. 5c and d).

## 4. Conclusions

*Fourier*-log and *Fourier*-ratio deconvolution techniques have been applied successfully to both low-loss and core-loss image-series. Experimental results show that deconvolution of core-loss series, in particular using the *Fourier*-log technique over an extended energy-loss range, can give an improvement in quantification and an increase in ionisation edge jump ratio. Further, the removal of plural scattering from the low-loss region allows the retrieval of low-loss edges for use in quantitative elemental mapping. The removal of plural scattering from EFTEM image-series should improve quantitative analysis of thicker specimens, improve the ability to separate overlapping ionisation edges and allow elemental maps to be obtained from low-lying edges normally obscured by multiple plasmon scattering.

## Acknowledgements

The authors would like to acknowledge the EPSRC and BNFL Magnox Generation for financial assistance. M. Weyland is thanked for the preparation of the steel sample used in this study.

## References

[1] J. Mayer, J.M. Plitzko, J. Microsc. 183 (1996) 2.
[2] P.J. Thomas, P.A. Midgley, Inst. Phys. Conf. Ser. 161 (1999) 239.
[3] P.J. Thomas, P.A. Midgley, Ultramicroscopy, preceding article in this issue, 88 (2001) 179.
[4] R.F. Egerton, Ultramicroscopy 3 (1978) 243.
[5] F. Hofer, G. Kothleitner, Microsc. Microanal. Microstruct. 4 (1993) 539.
[6] P.J. Thomas, P.A. Midgley, Proc. 14th ICEM, Cancun 1 (1998) 249.
[7] R.F. Egerton, M.J. Whelan, Philos. Mag. 30 (1974) 739.
[8] R.F. Egerton, Electron Energy Loss Spectroscopy in the Electron Microscope, 2nd Edition, Plenum Press, New York, 1996.
[9] G. Kothleitner, F. Hofer, Micron 29 (1998) 349.
[10] R.F. Egerton, Ultramicroscopy 9 (1982) 387.
[11] D.W. Johnson, J.C.H. Spence, J. Phys. D 7 (1974) 71.
[12] P.J. Thomas, P.A. Midgley, Proc. 12th EUREM, Brno 3 (2000) 309.
[13] Digital Micrograph software, © Gatan Inc. 66780 Owens Drive, Pleasanton, CA, 1992–2000.